Nanoscale

Cite this: *Nanoscale*, 2011, **3**, 5067

www.rsc.org/nanoscale

PAPER

Development of a mass-producible on-chip plasmonic nanohole array biosensor†

Kohei Nakamoto,[ab] Ryoji Kurita,[b] Osamu Niwa,*[ab] Toshiyuki Fujii[cd] and Munehiro Nishida*[e]

Received 20th July 2011, Accepted 27th September 2011
DOI: 10.1039/c1nr10883b

We have developed a polymer film based plasmonic device whose optical properties are tuned for measuring biological samples. The device has a circular nanohole array structure fabricated with a nanoimprint technique using a UV curable polymer, and then gold thin film is deposited by electron beam deposition. Therefore, the device is mass-producible, which is also very important for bioaffinity sensors. First the gold film thickness and hole depth were optimized to obtain the maximum dip shift for the reflection spectra. The dip shift is equivalent to the sensitivity to refractive index changes at the plasmonic device surface. We also calculated the variation in reflection spectra by changing the above conditions using the finite-difference time domain method, and we obtained agreement between the theoretical and experimental curves. The nanohole periodicity was adjusted from 400 to 900 nm to make it possible to perform measurements in the visible wavelength region to measure the aqueous samples with less optical absorption. The tuned bottom filled gold nanohole array was incorporated in a microfluidic device covered with a PDMS based microchannel that was 2 mm wide and 20 μm deep. As a proof of concept, the device was used to detect TNF-α by employing a direct immunochemical reaction on the plasmonic array, and a detection limit of 21 ng mL^{-1} was obtained by amplification with colloidal gold labeling instead of enzymatic amplification.

Introduction

Surface plasmons (SPs) are collective charge oscillations that are formed when light interacts with free electrons at a metal–dielectric interface. SPs have been studied in the field of plasmonics and are widely utilized for various applications including solar cells,[1] negative refractive index materials,[2] and medical diagnostic tools.[3] Because the excitation angles and wavelengths of SPs depend greatly on the surrounding dielectric environment, most SP based biosensors measure the refractive index change caused by a molecular interaction.[4] Surface plasmon resonance (SPR) biosensors play a particularly important role in drug screening technologies such as the BIAcore™ system and are expected to be a highly effective tool for clinical diagnosis since they facilitate label free and real-time measurements. The Kretschmann configuration is a well known optical setting for coupling evanescent waves with surface plasmons, and its simple optical system makes it possible to miniaturize the SPR sensors. We recently utilized a portable SPR sensor to construct a point of care testing (POCT) system.[5,6] By combining a microfluidic device and the portable SPR sensor, we successfully measured disease markers within 15 min in 50 μL of diluted urine samples.[7] However, an SPR biosensor based on the Kretschmann configuration requires a prism for plasmon excitation and a complicated sample chip setting by using such as matching oil between the prism and the sample chip. Recently, prism integrated SPR biosensing has been reported with the aim of developing disposable chips.[8] However, prism integration makes each chip much more expensive. Furthermore, it is difficult to construct a multi-analyte sensing system using a Kretschmann configuration and maintain portability. Although some researchers have realized SPR image devices for performing multiple biochemical tests, their systems require accurate and complicated optical setting and are expensive.[9,10]

Plasmonic sensors without any prisms for plasmon coupling have recently been demonstrated. They enable us to employ a simple optical setting such as localized surface plasmon resonance (LSPR) or a grating based plasmonic sensor by deploying gold or silver nano-structures.[11,12] Various plasmonic substrates with nanoparticle,[13] nanorod,[14] nanorice,[15] nanopyramid,[16] and

[a]*Institute of Materials Science, Graduate School of Pure and Applied Sciences, University of Tsukuba, 1-1-1 Tennodai, Tsukuba, 305-8573, Japan. E-mail: niwa.o@aist.go.jp*
[b]*National Institute of Advanced Industrial Science and Technology (AIST), Central 6, 1-1-1 Higashi, Tsukuba, 305-8566, Japan*
[c]*Graduate School of Integrated Arts and Sciences, Hiroshima University, Higashi-Hiroshima, 739-8521, Japan*
[d]*Research Institute for Science and Engineering, Waseda University, Shinjuku-ku, Tokyo, 169-8555, Japan*
[e]*Graduate School of Advanced Sciences of Matter, Hiroshima University, Higashi-Hiroshima, 739-8530, Japan. E-mail: mnishida@hiroshima-u.ac.jp*
† Electronic supplementary information (ESI) available. See DOI: 10.1039/c1nr10883b

nanoshell structures[17] have been investigated to obtain a strong electromagnetic field, because optical absorption or scattering derived from LSPR is strongly influenced by nanoparticle size, shape and packing density. Various LSPR sensor structures have exhibited sensitivity values ranging from roughly several tens to several hundreds of nm RIU^{-1}. Some plasmonic structures such as the nanograils reported by Heo *et al.* have exceeded 1000 nm RIU^{-1}.[18] However these values are far smaller than that of a conventional SPR with the Kretschmann configuration.

The key to realizing nanostructure based plasmonic devices that provide highly sensitive and accurate measurements is to fabricate uniform nanostructures on a substrate with a large area. Electron beam (EB) lithography or the focused ion beam (FIB) technique has been used to manufacture nanostructures so that the dimensions can be well controlled. However, these methods have a very low throughput because the fabrication is serial in nature so that large area samples take too long to fabricate. In addition, the above processes require large and expensive equipment.

More practical nanofabrication methods have been introduced that use a colloid arrangement as a mask for gold deposition or etching.[19,20] When the arranged colloids are used as a mask for gold deposition, a nano-order in triangular patterns is produced on the substrate, and this technique has been called nanosphere lithography (NSL)[21] by Van Duyne. The NSL method realizes plasmonic substrates with a greater than mm^2 scale. However, it is difficult to obtain defect free colloid surfaces. The NSL method is also limited in that it is mainly used to fabricate triangular structures.

On the other hand, colloidal lithography[22,23] is also a well known process that is employed when colloids are used as an etching mask.[23] For example, short-range ordered hole arrays have been successfully fabricated that are essentially defect free as reported by Dahlin and Sannomiya *et al.*[24–26] Colloidal lithography is a suitable process for fabricating such structures as regards simplicity, and cost. Also colloidal lithography has been used to manufacture long-range ordered hole structures. Masson *et al.* reported their realization of long-range nanohole structures with various periodicities by changing the colloid size.[27] However, an O_2 etching process is needed to obtain the desired hole diameter by adjusting the colloid diameter. In addition the hole order arrangements are limited to hexagonal patterns and it is also difficult to obtain defect free structures when we require sufficient surface area for multiple biosensing, although colloidal lithography can fabricate an essentially defect free surface for a relatively long-range order. Although Khanh and Yoon were able to align colloids in a square configuration by employing a method called "dry manual assembly", it requires accurate photolithographically fabricated template substrates.[28]

To overcome the limitation of the above processes, a nanoimprint technique has recently been introduced for fabricating plasmonic devices.[29] This top down process allows us to replicate defect free nanostructures precisely from an original mold with a size of several tens of nanometres over a large area. By changing the mold design, suitable configurations[30] for obtaining desired optical properties such as surface enhanced Raman spectroscopy (SERS),[31,32] LSPR and grating SPR can be fabricated. Molds can be used repeatedly and the technique is suitable for biosensing applications due to its inexpensive fabrication process. Nuzzo and Rogers' group fabricated periodical patterns consisting of sub-micron order round nanohole arrays by employing a soft nanoimprint technique with a flexible PDMS mold.[33,34] They also developed a bio-affinity sensor that had a spatial resolution of several microns by detecting transmission light passing through the substrate.[35] However, the nanohole patterns on the molds for plasmonic crystals were relatively large and deep (diameter $\approx$ 500 nm, depth $\approx$ 200 nm, periodicity $\approx$ 800 nm) compared with substrates reported by a different group.[36,37] In addition, their molds were based on PDMS, which is elastic and difficult to use to fabricate much smaller nanostructures with high precision. The SPR wavelength could be transferred from the near infrared region to the visible wavelength by fabricating a smaller nanohole array from robust material. The result would be that a simple optical setup could be used for biosensor applications. The transfer to the visible wavelength region would also enable us to avoid any overlap between the SPR dip and two water absorbance peaks observed around 970 and 1160 nm, and thus realize high peak resolution.

In this paper, we describe a simple and mass-producible plasmonic nanohole array device that can be employed to measure an immuno-reaction by optimizing the surface nanostructure using a UV nanoimprint method. We fabricated six kinds of mold patterns using a glassy carbon mold, which is cheaper than a nickel mold but more robust than a PDMS or Si mold. Accurate replication was obtained with no observable defects, and we realized a high correlation between refractive index and SPR wavelength. The highest sensitivity was obtained from a substrate with a hole depth of 50 nm, a periodicity of 600 nm, and a gold film thickness of 100 nm. This optimized nanostructure was also confirmed by 3D finite-difference time-domain (FDTD) simulations, which we employed to characterize the electromagnetic strength on the surface of the gold nanohole arrays. Finally, we covered our plasmonic device with a PDMS based straight microfluidic channel and used it to detect TNF-α *via* a real time immunoreaction.

Experimental

Materials

UV curable poly(urethane acrylate) (PUA) was obtained from Minuta Tech. (Seoul, Korea). Phosphate-buffered saline (PBS), pH 7.4, was purchased from Sigma Chemical Co. (St Louis, MO, USA). 10-Carboxy-1-decanethiol (10-CDT) was procured from Dojindo (Kumamoto, Japan). *N*-Hydroxysuccinimide (NHS) and *N*-ethyl-N¢-(3-dimethyl aminopropyl) carbodiimide hydrochloride (EDC) were purchased from Pierce (Rockford, IL, USA). 2-Aminoethanol and glycine were purchased from Nakalai Tesque, Inc. (Kyoto, Japan). Human tumor necrosis factor-α (TNF-α, human), anti-tumor necrosis antibody (mouse anti-TNF3/4), and biotinylated monoclonal anti-tumor necrosis antibody (mouse anti-TNF5) were purchased from MABTECH AB (Nacka Strand, Sweden). Streptavidin–gold was purchased from BioAssay Works (MD, USA). The gold particles coated with streptavidin are 40 nm in size. All the chemicals were analytical grade and were used as received.

Fabrication method

Fig. 1 shows the procedure for fabricating a bottom filled gold nanohole array by the nanoimprint technique. First, several microlitres of PUA prepolymer were dispensed onto glassy carbon (GC) molds with different size dots. After a poly(ethylene terephthalate) (PET) film with a thickness of 188 μm (Cosmo Shine A4300, Toyobo Co., Ltd) was put on PUA pre-polymer, a nanohole array pattern was replicated by curing PUA pre-polymer by exposure to ultraviolet (UV) light (EXECURE 4000-D, HOYA; Saitama, Japan) for 10 s. Subsequently, the PET film with the nanohole array was removed from the GC mold and rinsed in isopropyl alcohol and distilled water. Then various thicknesses of gold film were deposited on the substrate. A gold layer was selectively patterned on the substrates by employing an adhesive sheet with a 2 mm × 2 mm square hole by using electron beam evaporation (EB-680, Eiko Engineering, Tokyo, Japan). After the gold deposition, the adhesive sheet was removed. In the following sections, we call our substrate a "bottom filled gold nanohole array" to distinguish it from previously reported "gold nanohole arrays".

Measurement system

Our measurement system is shown in Fig. 2(a). We performed our measurement in the direct reflection mode. The optical system was constructed with a halogen light source (KBEX-051A), a spectrophotometer (S-2630) and a custom-made bundle fiber as shown in Fig. 2(a). The equipment was obtained from Soma Kogaku (Tokyo, Japan). The bundle fiber consists of ten optical fibers. One read fiber with a core diameter of 800 μm (NA = 0.22) is surrounded by nine illumination fibers with core diameters of 400 μm. Non-polarized light was illuminated and the reflected light was detected with a spectrometer. The reference spectrum was obtained from a flat gold surface surrounded by water. This is because we also observed reference reflection spectra from a mirror (TFA-25C05-10, Sigma Koki co., ltd. Tokyo, Japan) and confirmed that the difference of both spectra is small as shown in Fig. S10†. The detectable range of the spectrometer was from 400 to 900 nm. To measure the refractive index change on the nanohole array, the sample solution was placed on the nanohole array, which was then covered with a transparent glass plate (Matsunami; Osaka, Japan). Next, the nanohole array was illuminated with a vertical incident light from the light source *via* the optical fiber. The spectrum of light reflected from the nanohole array was monitored with the spectrometer, and recorded in a personal computer.

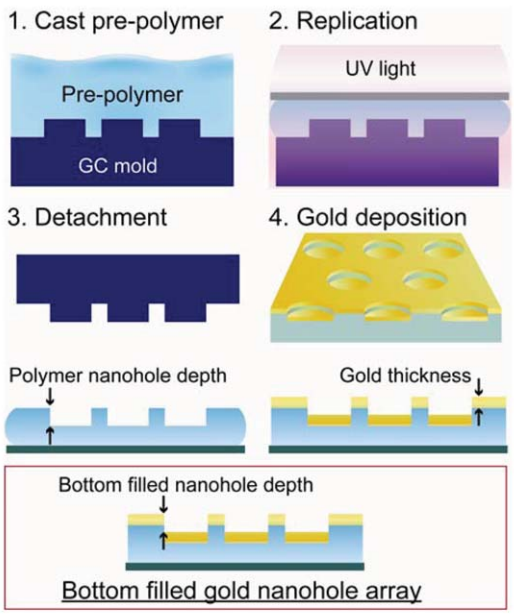

Fig. 1 Procedure for fabricating a gold nanohole array using the nanoimprint technique. First a UV curable oligomer was dropped into a glassy carbon mold. Then PET film was placed on the oligomer as a backing sheet. UV light was irradiated for about 10 seconds. The mold was then detached from the replicated substrate. After washing the substrate with ethanol and distilled water, various thicknesses of gold film were deposited on the nanohole arrays.

Immunoassay on bottom filled gold nanohole array

Fig. 2(b) and (c) show a photograph and a schematic of our SPR based immunosensor with a nanohole array. The immunoreaction surface was fabricated in a micro-flow channel using the following procedure. First, a self-assembled monolayer of carboxyl decanethiol was modified on the gold nanohole array by immersing 1 μM carboxyl decanethiol in ethanol for 2 hours. Anti-TNF-α antibody was then immobilized on the substrate by using the well-known carbodiimide coupling reaction provided by an EDC/NHS system.[6] We immersed the substrate with a carboxyl decanethiol monolayer in 10 mM acetate buffer (pH 5.0) that contained 0.4 mg mL^{-1} EDC and 1.1 mg mL^{-1} NHS. Then anti-TNF-α antibody was added to the buffer to give a final concentration of 20 μg mL^{-1} and the solution was incubated for 15 min at room temperature. BSA was then employed as a blocking material, and the substrates were covered with PDMS sheet that had a straight thin layer microchannel that was 2 mm wide, 10 mm long, and 20 μm deep. Two perfluoro(ethylene–propylene) plastic (FEP) tubes (BAS Inc., Tokyo, Japan) were connected to the inlet and outlet on the PDMS cover. A syringe pump (CMA102, Stockholm, Sweden) was connected to the other side of the tube connected to the outlet. All injection operations were conducted in the suction mode.

A schematic of the immunoassay technique is shown in Fig. 2 (d) and the detailed protocol is as follows. First, various concentrations of TNF-α were injected into the chip for 10 min (Fig. 2(d-1)). Subsequently, 1 μg mL^{-1} anti-TNF-α antibody-biotin was injected for 10 min. After rinsing the sensing surface with PBS buffer, 10 μg mL^{-1} streptavidin–gold was injected for 10 min. We measured the dip shift induced by the immuno- and biotin-streptavidin–gold reactions. All injection operations were undertaken using a syringe pump operating at a flow rate of 5 μL min^{-1}. All the experiments were performed at room temperature.

Results and discussion

Structural characterization of plasmonic nanohole arrays by AFM and SEM

Fig. 3 shows atomic force microscopy (AFM) images of nanohole arrays with depths of 50, 100, and 150 nm replicated by

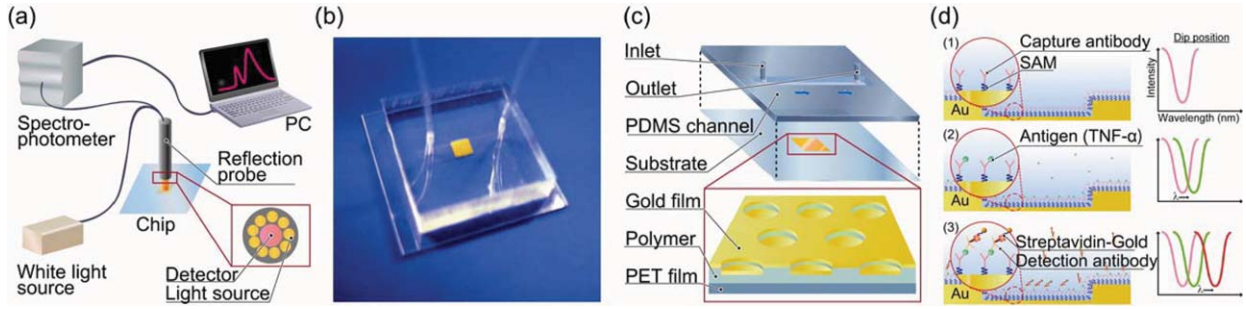

Fig. 2 (a) Measurement system for detecting the reflection spectrum from the substrate. The spectra are displayed on a PC after the reflection light has passed through a spectrophotometer. (b) Photo of the micro-sensing chip covered with PDMS with a straight channel that is 20 μm deep, 10 mm long, and 2 mm wide. (c) Schematic illustration of a plasmonic gold nanohole array chip. A pattern was formed on a thin PET film with an area of 2 mm × 2 mm. (d) Schematic illustration of an immunoassay process. (1) Capture antibody was immobilized by a carbodiimide coupling reaction on the gold nanohole array *via* self-assembled monolayers (SAMs). (2) Sample solution containing TNF-α was injected into the microchannel. All flow rates were 5 μL min^{-1}. (3) Streptavidin–gold was injected after the detection antibody was introduced. The SPR dip position was transferred to a longer wavelength by employing a bioaffinity reaction.

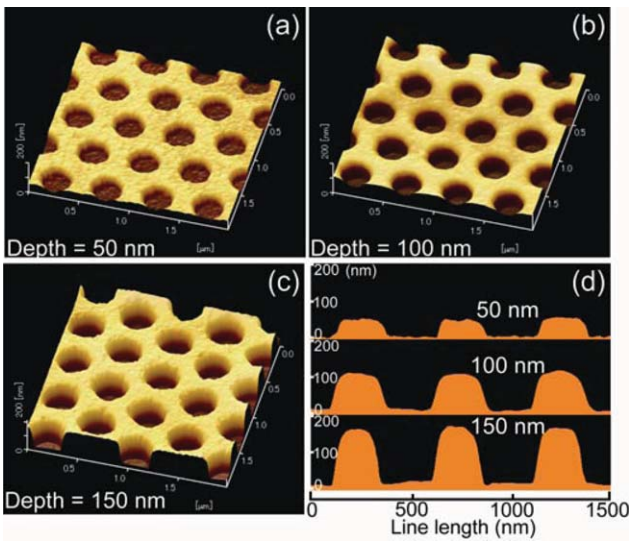

Fig. 3 Atomic force microscopy images of gold nanohole arrays with hole depths of (a) 50 nm, (b) 100 nm, and (c) 150 nm. (d) Line scans of each nanohole array.

glassy carbon molds with different designs. The mold patterns were successfully replicated on the substrate as shown in Fig. 3. The average surface roughness of a replicated substrate (4.95 nm) was about 15% less than that of a GC mold (6.29 nm). In addition, the nanohole array is accurately replicated independent of nanohole depth as shown in Fig. 3(d). The difference between the diameters of the bottom patterns of the mold and the replica is less than 10% from an AFM line scan.

We also observed replicated substrates with periodicities of 400, 500, 600, and 900 nm using a scanning electron microscope (SEM), as shown in Fig. 4. Nanoholes were successfully transferred without defects over large areas of up to 2 mm × 2 mm. Even after the nanoimprint procedure had been repeated more than 100 times, each mold maintained its initial shape and uniform structures could be replicated reproducibly. Each polymer nanohole array can be replicated within one minute with the nanoimprint technique as shown by the first three steps in Fig. 1 thus making it a suitable process for mass producing biosensors. In addition, a vacuum deposition process is used for fabricating commercial biosensors and so is potentially a high-throughput process.

Effect of gold thickness on plasmonic nanohole array sensor

Fig. 5(a) shows reflection spectra obtained from nanohole arrays with various gold film thicknesses. The nanohole array had a steady hole depth of 100 nm and a periodicity of 500 nm. Two distinctive dips (Dip1 and Dip2) were observed in the reflection spectra as seen in Fig. 5(a). Dip1 was sharper than Dip2. In addition, Dip1 almost maintained its sharpness when the gold thickness increased, however, Dip2 became broad and shallow. To interpret these two dips, we calculated reflectance, transmittance and absorption spectra from the gold nanohole array with or without a nanodisk in the bottom as described in ESI 7 (Fig. S7†). Fig. S7(a)† shows three kinds of spectra obtained from the gold nanohole array with a nanodisk in the bottom. When the first dip (Dip 1) was observed in the reflection spectrum, a clear peak was observed in the absorption spectrum. On the other hand, a second dip (Dip 2) was found in the reflection spectrum around 850 nm, and a peak was observed in the transmittance spectrum at almost the same wavelength. We also

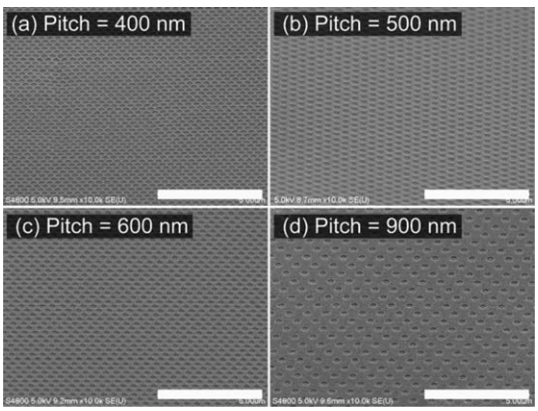

Fig. 4 Scanning electron microscope images of gold nanohole arrays with periodicities of (a) 400 nm, (b) 500 nm, (c) 600 nm, and (d) 900 nm. All bars are 5 μm.

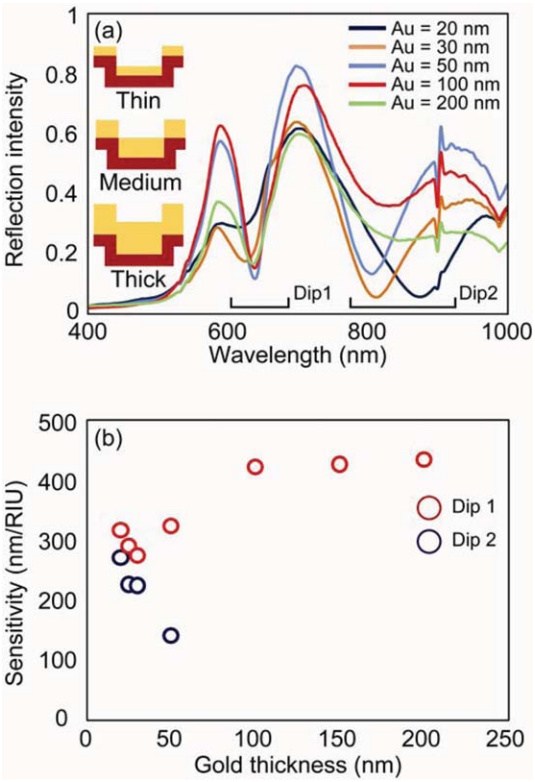

Fig. 5 (a) Reflection spectra with various gold thicknesses and (b) relationship between gold thickness and sensitivity.

calculated the values for a gold nanohole array without a nanodisk in the bottom and obtained the three kinds of spectra shown in Fig. S7(b)†. Two dips were observed in the reflectance spectrum at similar positions accompanied by the peak in the absorption spectrum for Dip 1 or in the transmittance spectrum for Dip 2 even if there was no nanodisk in the bottom. Thus Dip 1 is attributed to the Bloch wave surface plasmon polariton (SPP-BW) resonance, and Dip 2 is attributed to the local mode in the hole, that is, hole localized surface plasmon resonance (LSPR) as found in pure nanohole array systems without nanodisks discussed by Sannomiya *et al.*[25] From the time-averaged electric field distribution shown in ESI 8 (Fig. S8†), we infer that nanodisks play auxiliary roles in determining the shape of spectra by pushing the electric field to the top surface of the metal film for Dip 1, or cooperating with holes to guide the light transmission for Dip 2.

Fig. 5(b) shows the relationship between gold thickness and sensitivity towards changes in refractive index. When the gold thickness was 20 nm, the sensitivity of Dip1 was 316.01 nm RIU^{-1}, which was larger than that of Dip2 (270.28 nm RIU^{-1}). As the gold film thickness increased, the sensitivity of Dip1 increased. In contrast the sensitivity of Dip2 decreased. The highest sensitivity of 420 nm RIU^{-1} was obtained in Dip1 when the gold thickness was 200 nm. We focused on Dip1 in the following experiment because of its high sensitivity. With regard to gold thickness, we chose a 100 nm thick film for the following experiment. This is because a sharp SPR dip can be obtained when the gold film is thicker than 100 nm. However, the dip broadens when the thickness is increased to 200 nm. In contrast, the sensitivity to refractive index remains almost unchanged for thicknesses between 100 and 200 nm. A sharp SPR dip is advantageous for measuring a slight dip shift, which is important for obtaining high resolution. Therefore, 100 nm is the optimum thickness in terms of both sensitivity and resolution.

Effect of hole depth on SPR

We studied the effect of hole depth on SPR wavelength position, sharpness, and sensitivity towards the changes in refractive index as follows. We compare experimental and calculated results in Fig. 6. Three kinds of nanohole array structures were fabricated with depths of 50, 100, and 150 nm as shown in Fig. 6(a). Gold was deposited on each substrate to a thickness of 100 nm. From the experimental results, the sharpest peak was obtained when the hole depth was 50 nm. In addition, the resonance dip broadened with increasing hole depth. This could be because the existence of the exposed polymer substrate affects the SPR on the gold layer when the hole depth increases. In addition, it is more difficult to realize a uniform gold layer on the bottom surface when the hole depth increases (ESI 2†), resulting in a broad resonance dip. To further clarify the effect of hole depth on the SPR, we calculated three corresponding reflection spectra (depths of 50, 100 and 150 nm) and two more spectra (depths of 75 and 125 nm) using the three-dimensional finite-difference time domain (3D FDTD) method (Fig. S3†), which was based on the work of Nuzzo's group.[34] Although the basic trends of the dip sharpness and shift dependence on hole depth were roughly comparable, there were some differences when we compared experimental and simulated spectra together in one graph (red and blue lines in Fig. S4†). Therefore, we performed a further calculation by introducing another inverted cone structure that had a small bottom diameter of 250 nm based on the line scans obtained with AFM shown in Fig. 3. As a result, the dip position in the calculated results (green lines in Fig. S4†) became closer to that in the experimental results. Therefore, we could confirm that the simulated and experimental results for nanohole depth dependence show a very similar trend, although the match is still imperfect due to the side deposition of gold grains and the roughness of the gold film, as indicated in Fig. S2†.

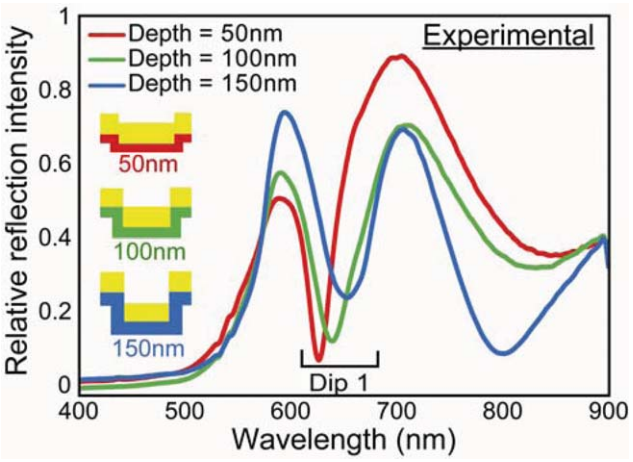

Fig. 6 Experimental results of relative reflection spectra from the gold nanohole arrays for hole depths of 50, 100, and 150 nm. Gold thickness is all same as 100 nm.

As shown in Fig. 6, the hole depth proved to be critical for obtaining a sharp SPR dip. To obtain a direct comparison of sensor sensitivity including the dip sharpness a previous study introduced a figure of merit (FOM) expressed as follows:[38,39]

$$\mathrm{FOM} = \frac{S(\mathrm{nm/RIU})}{\mathrm{fwhm(nm)}} \quad (1)$$

Here, S is the linear slope for the refractive index and FWHM is the full width at half maximum of a dip. The refractive index slope S was experimentally estimated by a linear fitting of the dip wavelength shift and the surface refractive indices. Table 1 shows a summary of results estimated from Fig. 6(a). The FOM values for our nanohole array were 14.3, 9.4, and 8.2 for depths of 50, 100, and 150 nm, respectively. Although a substrate with hole depth of 150 nm has a 1.037 times larger S than that of a substrate with a hole depth of 50 nm, the latter has the lowest FWHM of 28.7 nm, which is about half that of the former. Therefore, a substrate with a hole depth of 50 nm realizes the highest FOM of 14.3 as shown in Table 1. This value is about three times higher than that obtained with a nanoparticle based plasmonic substrate.[16]

Murray-Méthot *et al.* have previously reported a method for evaluating the FH/FWHM calculation.[40] They revealed the spectral resolution by introducing FH/FWHM (full height/full width at half maximum). We also displayed the FH/FWHM values of each substrate in Table 1. We obtained the same descending order of FH/FWHM as obtained for the FOM value. But, our highest value is about 16 times higher than that reported by Murray-Méthot. Based on these results, we utilized substrates with hole depths of 50 nm in the following experiment.

Effect of periodicity on plasmonic nanohole array sensor

Next we varied the nanohole periodicity from 400 to 900 nm while maintaining a hole depth of 50 nm and a gold thickness of 100 nm as shown in Fig. 7. The slopes in Fig. 7(a) become steep as the periodicity increases. This indicates that the sensitivity can be improved by increasing the periodicity. However, an SPR dip with 900 nm periodicity was not observed because the inferred dip position was beyond the range of the spectrometer. The demonstrated sensitivities for each periodicity were 300.2, 419.2, and 495.0 (nm RIU^{-1}), respectively. When we compare the experimental results obtained for refractive index change and dip wavelength with the calculated results, there is a good agreement between them as shown in ESI 5†. Our sensitivity is about 7 times larger than that obtained from gold colloids (66.5 nm RIU^{-1}), and 1.5 times larger than that of a gold nanohole substrate made using EB lithography (333 nm RIU^{-1})[41] or colloidal lithography (300 nm RIU^{-1}).[42] Here we express the sensitivity S of our triangular gold nanohole substrate as follows:

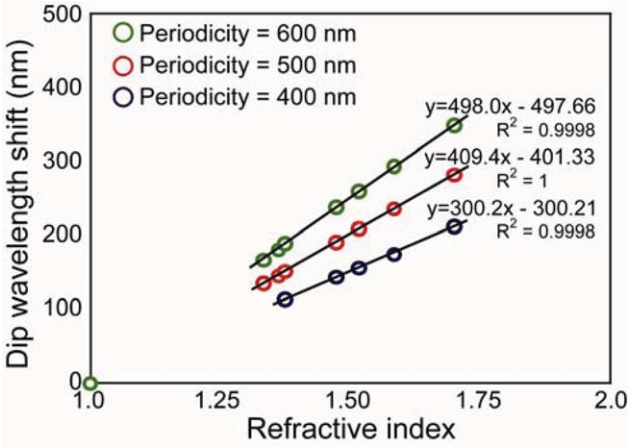

Fig. 7 Dependence of the plasmon resonance dip wavelength shift on the refractive index when the reflection spectra were obtained from gold nanohole arrays with periodicities of 400, 500 and 600 nm.

$$S = \frac{\mathrm{d}\lambda}{\mathrm{d}n} = \frac{\sqrt{3}}{2}\frac{d}{\sqrt{p^2+q^2-pq}}\sqrt{\left(\frac{\varepsilon_{\mathrm{Au}}}{\varepsilon_{\mathrm{Au}}+n^2}\right)^3} \quad (2)$$

Here, λ is the wavelength of the dip position, n is the refractive index, d is the periodicity, p and q are the grating orders, and $\varepsilon_{\mathrm{Au}}(\omega)$ is the dielectric constant. This equation was derived from the lattice vector equation and the wave number of the surface plasmon polariton. The appendix provides more detail. According to eqn (2), S correlates with d when the dielectric constant of gold and the surrounding refractive index are steady. In fact, the relationship between S and d calculated from our experimental results shown in Fig. 7(a) is expressed as follows:

$$S = 0.9889d - 94.58\ (R^2 = 0.9995) \quad (3)$$

As Pang *et al.* reported,[43] a high sensitivity of 1520 nm RIU^{-1} in the (1, 0) SPP mode is observed when the nanohole array has a periodicity of 1530 nm. This result correlates with eqn (3) obtained from our experimental results. A high sensitivity is desired for biosensors, but the SPR dip shifted into the infrared region (~1533 nm). This requires a more expensive experimental setup than that used for detecting an SPR dip at visible wavelengths. Moreover, water absorption in the infrared red region reduces the sensitivity, which is unsuitable for a low cost biosensor. Oh's group reported a sensitivity of 600 nm RIU^{-1} for a double nanohole array.[44] This study encourages us to obtain a higher sensitivity at visible wavelengths by making such structures with a simpler method using a nanoimprint technique.

The FOM of gold nanohole arrays with periodicities of 400, 500, and 600 nm were estimated to be 9.4, 14.3 and 20.2,

Table 1 Comparison of figures of merit (FOM) and FH/FWHM values of gold nanohole substrates with hole depths of 50, 100 and 150 nm

Hole depth/nm	Sensitivity/nm RIU^{-1}	FWHM/nm	FOM	FH	(FH/FWHM)/nm^{-1}
50	409.44	28.7	14.27	0.56	19.6×10^{-3}
100	419.15	44.4	9.44	0.61	13.8×10^{-3}
150	424.57	51.9	8.18	0.59	11.3×10^{-3}

respectively. Although each value of FWHM was almost same (see ESI Fig. S1†), substrates with a periodicity of 600 nm exhibited the highest FOM number due to high sensitivity. This value is higher than that of previous plasmonic sensors such as silver nanocubes (FOM = 5.4),[45] nanowell surfaces fabricated by nanosphere lithography (FOM = 14.5),[21] and nanobipyramids formed by solution phase synthesis (FOM = 4.5).[16] Odom *et al.* reported a very high FOM value of about 80 when Ag was used as the surface metal and the incident light angle was 64 deg.[46] SPR on Ag is known to exhibit a sharp peak compared with SPR on Au; however Ag is unstable owing to surface oxidation in air. Our SPR on a Au nanoarray is stable against oxidation. In addition, we can simply measure the spectra by using the vertical irradiation of an incident light without tuning its angle.

Typical reflection spectra from gold nanohole array

Fig. 8(a) shows the normalized reflection SPR spectra for various bulk refractive indices at a hole depth of 50 nm, a periodicity of 600 nm and a gold thickness of 100 nm. The dip shifted to a longer wavelength in response to solutions with an increased refractive index. Our device can detect a wide range of refractive indices from 1.000 (air) to 1.700 (matching oil) as shown in Fig. 8 (b). Also, with our sensor there is a linear relation between the bulk refractive index change and the relative SPR wavelength shift with a high correlation coefficient of 0.9998, which quantitative interpretation could be simplified. When the solution was changed, the gold surfaces were carefully washed with ethanol and distilled water. When we employed distilled water after detecting matching oil with a refractive index of 1.70, the dip position shifted to the first detection point of the distilled water, resulting in good reproducibility. In this experiment, we measured reflection spectra through the sample solution. However the measurement of reflection spectra without sample solution is also possible, realizing that we can employ the measurement with non-transparent samples after removing the sample solution from the sensing area.

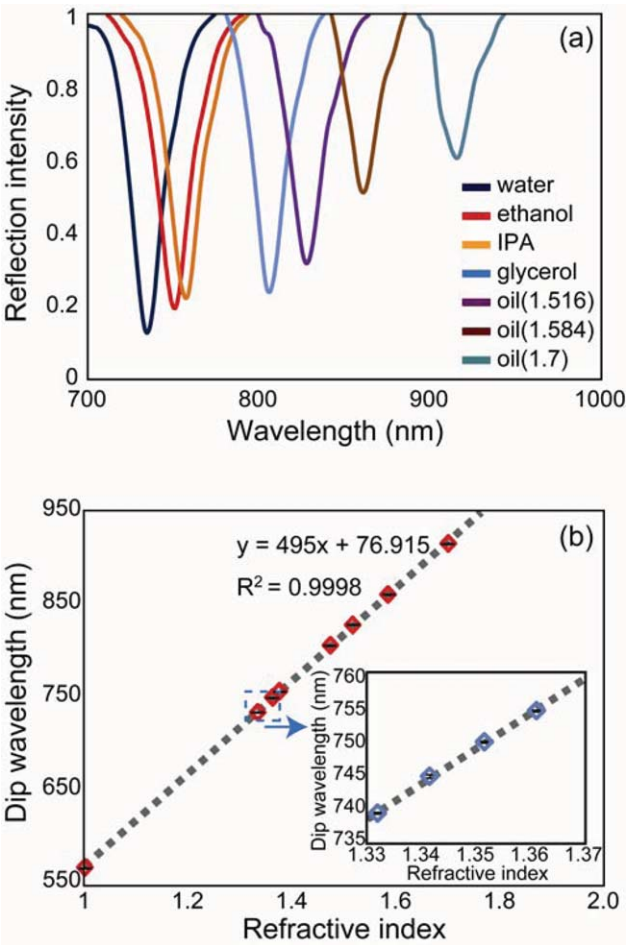

Fig. 8 (a) Reflection spectra from a gold nanohole array with a periodicity of 600 nm, a diameter of 300 nm, a depth of 50 nm, and a gold thickness of 100 nm when the surface was surrounded by various refractive indices. (b) Dip wavelength dependence on the refractive index of the substrate.

Immunoassay on gold nanohole array

To evaluate the device, we conducted an immunoassay employing our plasmonic gold nanohole array integrated with a microfluidic device. Reflection mode measurement is a convenient and suitable approach for simple biosensing because the probe fiber illuminates and collects from the same side. Watanabe *et al.* reported LSPR sensing using the same optical setting[21,47,48] with a smaller core diameter of 62.5 μm compared with ours of 800 μm. This is because we aim to fabricate multiple biosensing chips with good reproducibility based on the current reflection measurement mode. We have to use a relatively large sensing area since it is difficult to immobilize biomolecules reproducibly in a small area. By constructing a millimetre order detection area for capture probe modification, we can realize a more accurate measurement technique. We used a nanohole array with a diameter of 300 nm, a depth of 50 nm, a periodicity of 600 nm, and a gold thickness of 100 nm. A capture antibody was immobilized on the gold surface, resulting in a relative dip wavelength red shift of about 1.2 nm as shown in Fig. 9(a). Fig. 9 (b) shows a calibration curve for TNF-α. The real-time measurement results are shown in Fig. S9†. A shift in the SPR dip towards a longer wavelength was observed as the TNF-α concentration increased within 10 min for conventional immunoreactions with ng mL^{-1} level TNF-α, which is consistent with the formation of an immuno-complex on the nanohole array. Subsequently we injected the secondary antibody and streptavidin–gold solution into the chip. After injecting 10 μg mL^{-1} of secondary antibody solution, the dip shifted to wavelengths that were about 0.5 nm (1 μg mL^{-1} antigen) and 0.2 nm (100 ng mL^{-1} antigen) longer. No relative shift was observed when the antigen concentration was less than 10 ng mL^{-1}. However, we observed a large wavelength shift by injecting 10 μg mL^{-1} of streptavidin–gold solution for 10 min after injecting 10 ng mL^{-1} of antigen solution. This is because a number of Au colloids were trapped on the nanohole array by the biotin–avidin interaction, which was confirmed from SEM images as shown in the inset of Fig. 9(b). The detection limits, which were defined from three times the standard deviation of negative control at direct immunoreactions and streptavidin–gold reaction, were 0.1 and 0.32, respectively. From these values, we estimated a detection limit of 21 ng mL^{-1} using streptavidin–gold and 45 ng mL^{-1}

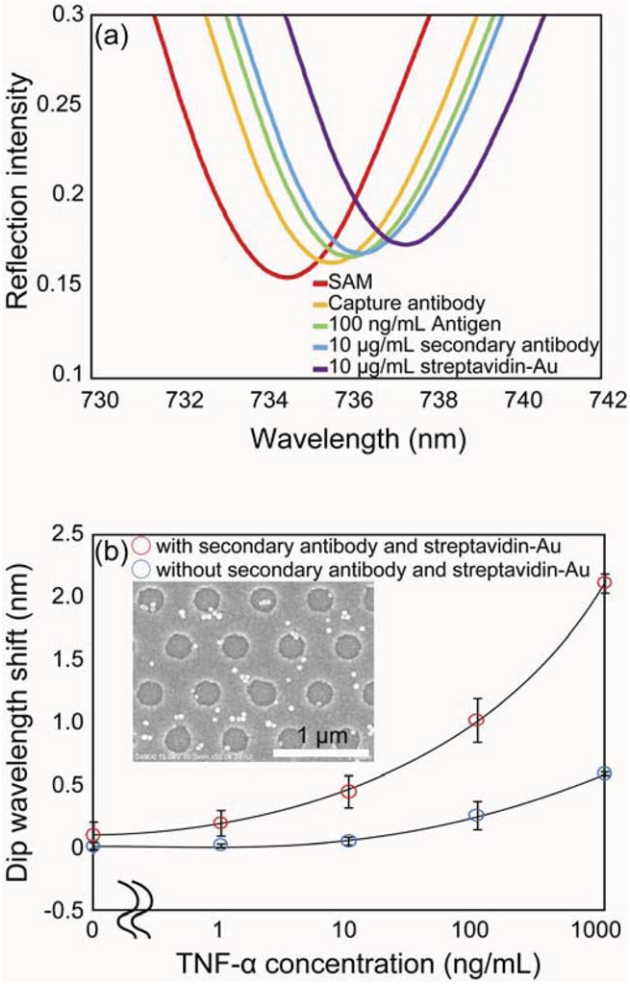

Fig. 9 (a) Reflection spectra when we modified self-assembled monolayers (red), capture antibody (orange), reacted with antigen (green), secondary antibody (blue), and streptavidin–gold (purple). (b) Calibration curve for immunoassay between anti anti-TNF α antibody and TNF-α with (red) or without (blue) streptavidin–gold. All flow rates were 5 μL min^{-1}. (Inset) SEM image of the gold nanohole array with streptavidin gold.

with direct immunoassay. By injecting streptavidin–gold, the detection limit for TNF-α was improved about 2.1 times compared with the result obtained without the streptavidin–gold injection. Eddings *et al.* reported that 120 ng mL^{-1} IgG was detected without labeling by using Flexchip with a flow rate of 300 μL min^{-1}. Our value without labeling streptavidin–gold constitutes a threefold improvement compared with the value obtained using Flexchip. Our polymer based device and the above performance characteristics such as the detection limit suggest that our device could be used as a platform on which to develop various biosensors for clinical tests.

Conclusion

We developed a plasmonic nanohole array sensor using the UV nanoimprint technique. We studied the influence of various parameters of the nanohole array structure on the refractive index change by tuning the hole depth topography, gold deposition thickness and hole periodicity. With regard to the hole depth, we obtained corresponding simulated spectra to allow us to study the trend. As a result, we determined that a nanohole array with a depth of 50 nm, a periodicity of 600 nm, and a gold thickness of 100 nm exhibited the largest sensitivity, which makes it suitable for biosensor applications. We employed the nanohole with the optimized design for an immunoassay of TNF-α by combining it with a PDMS based microchannel and achieved a detection limit of 21 ng mL^{-1} with streptavidin gold labeling and of 45 ng mL^{-1} without labeling, respectively. The latter detection limit obtained without labeling is still about three times lower than that obtained by Flexchip. We believe that our sensor has the potential for use as a practical point of care testing sensor chip.

Appendix

We describe the sensitivity in order to characterize our results and compare previous work with the following calculations. The wave number of a surface plasmon polariton (k_{spp}) is usually expressed as

$$k_{SPP} = \frac{\omega}{c}\sqrt{\left(\frac{\varepsilon_{Au}(\omega)n^2}{\varepsilon_{Au}(\omega)+n^2}\right)} \quad (4)$$

where, ω is angular frequency, n is the refractive index of the sample solution, and $\varepsilon_{Au(\omega)}$ is the dielectric constant. When the light is illuminated vertically, there is no wave number parallel to the triangular lattice. Thus, the wave number vector is limited to the reciprocal lattice vector $\boldsymbol{G}$. The amount of $\boldsymbol{G}$ is shown as follows:

$$G = \frac{4\pi}{\sqrt{3}d}\sqrt{p^2+q^2-pq} \quad (5)$$

where d is the periodicity of the nanohole array, and p and q are the grating orders. When the wavelength of the incident light satisfies the following equation where k_{SPP} and G are equal, an absorbance peak appears that is derived from the surface plasmon resonance:

$$\frac{4\pi}{\sqrt{3}d}\sqrt{p^2+q^2-pq} = \frac{\omega}{c}\sqrt{\left(\frac{\varepsilon_{Au}(\omega)n^2}{\varepsilon_{Au}(\omega)+n^2}\right)} \quad (6)$$

Under this condition, the incident light wavelength, λ, is expressed as follows:

$$\lambda = \frac{\sqrt{3}}{2}\frac{d}{\sqrt{p^2+q^2-pq}}\sqrt{\left(\frac{\varepsilon_{Au}(2\pi c/\lambda)n^2}{\varepsilon_{Au}(2\pi c/\lambda)+n^2}\right)} \quad (7)$$

From eqn (7), the sensitivity S is expressed as follows:

$$S = \frac{d\lambda}{dn} = \frac{\sqrt{3}}{2}\frac{d}{\sqrt{p^2+q^2-pq}}\sqrt{\left(\frac{\varepsilon_{Au}}{\varepsilon_{Au}+n^2}\right)^3} \quad (8)$$

Acknowledgements

We thank N. Hatakenaka for fruitful discussions regarding electromagnetic calculations related to our device. This work was supported by a Grant-in-Aid for challenging Exploratory Research (no. 23651149), Research Fellowships of the Japan Society for the Promotion of Science for Young Scientists (no.

21-3300) and a Grant-in-Aid for Young Scientists (B) (no. 20710104). Part of this work was conducted at the Nano-Processing Facility, supported by the IBEC Innovation Platform, AIST.

References

1 E. Moulin, P. Q. Luo, B. Pieters, J. Sukmanowski, J. Kirchhoff, W. Reetz, T. Muller, R. Carius, F. X. Royer and H. Stiebig, *Appl. Phys. Lett.*, 2009, **95**, 033505.
2 W. Wu, Z. N. Yu, S. Y. Wang, R. S. Williams, Y. M. Liu, C. Sun, X. Zhang, E. Kim, Y. R. Shen and N. X. Fang, *Appl. Phys. Lett.*, 2007, **90**, 063107.
3 J. Zhao, X. Y. Zhang, C. R. Yonzon, A. J. Haes and R. P. Van Duyne, *Nanomedicine*, 2006, **1**, 219–228.
4 J. Homola, *Chem. Rev.*, 2008, **108**, 462–493.
5 K. Nakamoto, R. Kurita, N. Sekioka and O. Niwa, *Chem. Lett.*, 2008, **37**, 698–699.
6 R. Kurita, Y. Yokota, Y. Sato, F. Mizutani and O. Niwa, *Anal. Chem.*, 2006, **78**, 5525–5531.
7 K. Nakamoto, R. Kurita and O. Niwa, *Biosens. Bioelectron.*, 2010, **26**, 1536.
8 S. J. Kim, K. V. Gobi, H. Iwasaka, H. Tanaka and N. Miura, *Biosens. Bioelectron.*, 2007, **23**, 701–707.
9 Y. Iwasaki, T. Tobita, K. Kurihara, T. Horiuchi, K. Suzuki and O. Niwa, *Biosens. Bioelectron.*, 2002, **17**, 783–788.
10 B. P. Nelson, T. E. Grimsrud, M. R. Liles, R. M. Goodman and R. M. Corn, *Anal. Chem.*, 2001, **73**, 1–7.
11 M. E. Stewart, C. R. Anderton, L. B. Thompson, J. Maria, S. K. Gray, J. A. Rogers and R. G. Nuzzo, *Chem. Rev.*, 2008, **108**, 494–521.
12 J. N. Anker, W. P. Hall, O. Lyandres, N. C. Shah, J. Zhao and R. P. Van Duyne, *Nat. Mater.*, 2008, **7**, 442–453.
13 S. Nishiuma, Y. Handa, T. Imamura, M. Ogino, T. Yamada, K. Furusawa and R. Kuroda, *Jpn. J. Appl. Phys.*, 2008, **47**, 1828–1832.
14 H. Nakashima, K. Furukawa, Y. Kashimura and K. Torimitsu, *Langmuir*, 2008, **24**, 5654–5658.
15 H. Wang, D. W. Brandl, F. Le, P. Nordlander and N. J. Halas, *Nano Lett.*, 2006, **6**, 827–832.
16 H. J. Chen, X. S. Kou, Z. Yang, W. H. Ni and J. F. Wang, *Langmuir*, 2008, **24**, 5233–5237.
17 T. Endo, K. Kerman, N. Nagatani, Y. Takamura and E. Tamiya, *Anal. Chem.*, 2005, **77**, 6976–6984.
18 C. J. Heo, S. H. Kim, S. G. Jang, S. Y. Lee and S. M. Yang, *Adv. Mater.*, 2009, **21**, 1726.
19 L. S. Live and J. F. Masson, *J. Phys. Chem. C*, 2009, **113**, 10052–10060.
20 L. S. Live, O. R. Bolduc and J. F. Masson, *Anal. Chem.*, 2010, **82**, 3780–3787.
21 E. M. Hicks, X. Y. Zhang, S. L. Zou, O. Lyandres, K. G. Spears, G. C. Schatz and R. P. Van Duyne, *J. Phys. Chem. B*, 2005, **109**, 22351–22358.
22 A. Dahlin, M. Zach, T. Rindzevicius, M. Kall, D. S. Sutherland and F. Hook, *J. Am. Chem. Soc.*, 2005, **127**, 5043–5048.
23 M. Roca, N. H. Pandya, S. Nath and A. J. Haes, *Langmuir*, 2010, **26**, 2035–2041.
24 A. B. Dahlin, S. Chen, M. P. Jonsson, L. Gunnarsson, M. Kall and F. Hook, *Anal. Chem.*, 2009, **81**, 6572–6580.
25 T. Sannomiya, O. Scholder, K. Jefimovs, C. Hafner and A. B. Dahlin, *Small*, 2011, **7**, 1653–1663.
26 M. P. Jonsson, A. B. Dahlin, P. Jonsson and F. Hook, *Biointerphases*, 2008, **3**, Fd30–Fd40.
27 J. F. Masson, M. P. Murray-Méthot and L. S. Live, *Analyst*, 2010, **135**, 1483–1489.
28 N. N. Khanh and K. B. Yoon, *J. Am. Chem. Soc.*, 2009, **131**, 14228.
29 A. Boltasseva, *J. Opt. A: Pure Appl. Opt.*, 2009, **11**, 2199–2203.
30 B. D. Lucas, J. S. Kim, C. Chin and L. J. Guo, *Adv. Mater.*, 2008, **20**, 1129–1134.
31 A. J. Baca, T. T. Truong, L. R. Cambrea, J. M. Montgomery, S. K. Gray, D. Abdula, T. R. Banks, J. M. Yao, R. G. Nuzzo and J. A. Rogers, *Appl. Phys. Lett.*, 2009, **94**, 243109.
32 R. Alvarez-Puebla, B. Cui, J. P. Bravo-Vasquez, T. Veres and H. Fenniri, *J. Phys. Chem. C*, 2007, **111**, 6720–6723.
33 J. M. Yao, M. E. Stewart, J. Maria, T. W. Lee, S. K. Gray, J. A. Rogers and R. G. Nuzzo, *Angew. Chem., Int. Ed.*, 2008, **47**, 5013–5017.
34 M. E. Stewart, N. H. Mack, V. Malyarchuk, J. A. N. T. Soares, T. W. Lee, S. K. Gray, R. G. Nuzzo and J. A. Rogers, *Proc. Natl. Acad. Sci. U. S. A.*, 2006, **103**, 17143–17148.
35 M. E. Stewart, J. M. Yao, J. Maria, S. K. Gray, J. A. Rogers and R. G. Nuzzo, *Anal. Chem.*, 2009, **81**, 5980–5989.
36 R. Gordon, M. Hughes, B. Leathem, K. L. Kavanagh and A. G. Brolo, *Nano Lett.*, 2005, **5**, 1243–1246.
37 A. G. Brolo, S. C. Kwok, M. G. Moffitt, R. Gordon, J. Riordon and K. L. Kavanagh, *J. Am. Chem. Soc.*, 2005, **127**, 14936–14941.
38 E. M. Hicks, O. Lyandres, W. P. Hall, S. L. Zou, M. R. Glucksberg and R. P. Van Duyne, *J. Phys. Chem. C*, 2007, **111**, 4116–4124.
39 M. A. Otte, B. Sepulveda, W. H. Ni, J. P. Juste, L. M. Liz-Marzan and L. M. Lechuga, *ACS Nano*, 2010, **4**, 349–357.
40 M. P. Murray-Méthot, M. Ratel and J. F. Masson, *J. Phys. Chem. C*, 2010, **114**, 8268–8275.
41 A. De Leebeeck, L. K. S. Kumar, V. de Lange, D. Sinton, R. Gordon and A. G. Brolo, *Anal. Chem.*, 2007, **79**, 4094–4100.
42 V. Canpean and S. Astilean, *Lab Chip*, 2009, **9**, 3574–3579.
43 L. Pang, G. M. Hwang, B. Slutsky and Y. Fainman, *Appl. Phys. Lett.*, 2007, **91**, 123112.
44 A. Lesuffleur, H. Im, N. C. Lindquist and S. H. Oh, *Appl. Phys. Lett.*, 2007, **90**, 243110.
45 L. J. Sherry, S. H. Chang, G. C. Schatz, R. P. Van Duyne, B. J. Wiley and Y. N. Xia, *Nano Lett.*, 2005, **5**, 2034–2038.
46 H. W. Gao, J. Henzie, M. H. Lee and T. W. Odom, *Proc. Natl. Acad. Sci. U. S. A.*, 2008, **105**, 20146–20151.
47 K. Kajikawa, K. Mitsui and Y. Handa, *Appl. Phys. Lett.*, 2004, **85**, 4231–4233.
48 K. Kajikawa and M. Watanabe, *Sens. Actuators, B*, 2003, **89**, 126–130.